

EXPERIMENTAL CHARACTERIZATION OF THE DIMENSIONLESS MOMENTUM LENGTH FOR SUBMERGED JET DISCHARGES OF AIR-STEAM MIXTURES INTO STAGNANT WATER

Y. CÓRDOVA^{1,2}, D. BLANCO¹, C. BERNA¹, J.L. MUÑOZ-COBÓ¹, A. ESCRIVÁ¹ & Y. RIVERA¹

¹ Instituto de Ingeniería Energética, Universitat Politècnica de València, Spain.

² Instituto Superior de Tecnologías y Ciencias Aplicadas, Universidad de La Habana, Cuba.

ABSTRACT

A very efficient method of condensing the steam in various industrial applications is the steam direct discharge into pools with subcooled water. This kind of condensation is known as Direct Contact Condensation (DCC), by providing high heat transfer and mass exchange capacity, the steam condenses quickly. In the past few decades, many experiments have been carried out on the submerged jets of non-condensable gases and pure steam in pools, supplying much information of interest, but efforts are still being made to obtain more information. In particular, the research of steam and non-condensable gas mixtures is of great interest to the chemical, energy, and nuclear industry. Consequently, this study investigates the discharge behavior of air-steam mixtures in a pool with subcooled water by direct visualization techniques using a high-speed camera. To know the behavior of the dimensionless momentum length, tests were carried out considering several initial discharge conditions such as nozzle diameter, percentage of mixture, and flow rates. After image acquisition, a series of complex processing, filtering, and post-processing procedures are applied using a subroutine in MATLAB. The momentum length of the jet was measured and found to be heavily influenced by the nozzle diameter, the jet velocity, and the mixture percentage. A correlation is obtained for the dimensionless momentum length of the horizontal jet that depends on the Froude and Mach numbers.

Keywords: jets, air-steam mixture, direct contact condensation, dimensionless momentum length, digital image processing

1 INTRODUCTION

DCC phenomenon of steam in the presence of non-condensable gases is of great interest for the nuclear industry, as it performs a critical role in the design of the safety system incorporated in the Boiling Water Reactors (BWR). In a possible loss-of-coolant accident (LOCA) of a BWR, a large amount of steam and non-condensable gases are injected into the pressure suppression pool (SP). This process is extremely important because it can alleviate the threat of containment overpressure and fission product release. In the first blowdown, after vents cleaning, the concentration of non-condensable gas is reduced from 100% to less than 10%, followed by a longer steam injection occurs [1].

Two methods are mainly used to analyze the interface characteristics of the jet immersed in the supercooled water. The first to use visualization-based measurement techniques to study the behavior of the gas–liquid interface, jet profile, bubble collapse and bubble behavior. Another method involves measuring the parameters of the flow field, including temperature, dynamic pressure and sound signals. Among the two methods, the first method is the most widely used because it does not interfere with the flow field.

To characterize the condensation of a steam jet discharged in sub-cooled water, one of the key points is the penetration length of the steam plumes. Two methods are mainly applied to investigate submerged jet interface characteristics in the subcooled water. The first uses visualization-based measurement techniques to study the liquid–gas interface behavior, the jet contour, bubble breakup and bubble behavior. Another method involves measuring the parameters of the flow field, including dynamic pressure, sound signals and temperature. Of the two methods, the first is the most widely used as it does not disturb the flow field. This method can be divided into two groups: direct visualization techniques (cameras incorporating charge-coupled devices (CCD) and illumination systems are used) and advanced visualization techniques (laser systems are used as an illumination source).

Stanford and Webster [2] concluded that the penetration length of the steam plume was directly proportional to the natural logarithm of the steam mass flow rate. However, the Stanford and Webster correlation does not predict the experimental data from other studies. Kerney *et al.* [3] developed a simplified, but more general, approach to computing the dimensionless penetration length of the steam plume. They assumed that the transport modulus and critical steam mass flux at ambient pressure were constant values in the semiempirical penetration length correlation. This correlation has been widely used by other researchers in recent decades, Chun *et al.* [4], Kim *et al.* [5], Sun *et al.* [6] and Meng *et al.* [7]; these have adaptively modified the correlation fit coefficients according to their measurements. Weimer *et al.* [8] suggested a more complex model, which considered the behavior of various liquid fluids, obtaining a correlation of the penetration length that further depended on the density ratio but redefined the value of condensation driving potential. Wu *et al.* [9] defined a correlation that depended on the relation of the steam pressure at the nozzle exit and the pressure conditions where the jet was discharged, because they noticed in their experiments a strong dependence of the shape of the supersonic steam plume on the pressure. Subsequently, Chong *et al.* [10] experimentally compared two types of nozzles with different structure and obtained a correlation that depended on the maximum expansion ratio. According to the experimental data obtained by Qiu *et al.* [11], they performed a penetration length correlation considering water temperature, steam mass flow rate and pressure ratio for a supersonic steam discharge. In place of using the relation of steam mass flow to its average value, Wang *et al.* [12] preferred to fitting their experimental data of the supersonic steam jet with a correlation as a function of Mach number. Table 1 shows the previous correlations for momentum length.

As shown so far, all penetration length correlations refer to pure steam jets. This is determined by the complexity of performing experiments that are mixtures of non-condensable gases and steam, because the presence of non-condensable gases deteriorates heat transfer and affects steam condensation. The only research that obtains a correlation that considers the influence of noncondensable gases is Li *et al.* [13]. In this research, a dimensionless penetration length correlation was obtained for a horizontally discharged jet that depended on the Froude number and the air mass fraction.

Related to non-condensable gas discharges, some correlations have been obtained, as are the case in the investigations of Igwe [14], Hoefele [15], Carreau [16], Emani [17], Harby *et al.* [18] and Rassame *et al.* [19]. These correlations are expressed as function of a modified Froude number.

The objective of the present paper is to contribute to expand the scarce database of steam and non-condensable gas mixtures discharges currently available. To this end, we focus on characterizing the behavior of the horizontally discharged jet, the effect of air volumetric

Table 1: Previous correlations for momentum length of horizontally discharged steam jet.

Researchers	Momentum length (L/D)	Definition of B
Kerney <i>et al.</i> (1972)	$C_1 \cdot B^{C_2} (G/G_m)^{C_3}$	$c_p (T_{sat} - T_f)/h_{fg}$
Chun <i>et al.</i> (1996)	$C_1 = 0.7166$, $C_2 = 0.1689$ and $C_3 = 0.6446$	
Kim <i>et al.</i> (2001)	$C_1 = 0.5923$, $C_2 = -0.66$ and $C_3 = 0.3444$	
Sun <i>et al.</i> (2018)	$C_1 = 0.503$, $C_2 = -0.70127$ and $C_3 = 0.47688$	
Meng <i>et al.</i> (2019)	$C_1 = 0.116$, $C_2 = -1.19$ and $C_3 = 0.9$ $C_1 = 0.1776$, $C_2 = -1.0327$ and $C_3 = 0.9594$	
Weimer <i>et al.</i> (1973)	$17.75B^{-1} (G/G_{ee})^{0.5} (\rho_f/\rho_{ee})^{-0.5}$ $10.285B^{-0.801} (G/G_{ee})^{0.713} (\rho_f/\rho_{ee})^{-0.384}$	$(h_f - h_\infty)/(h_{ee} - h_f)$
Wu <i>et al.</i> (2007)	$0.868B^{-0.6} (G/G_m)^{0.5} (\rho_s/\rho_\infty)^{0.2}$	$c_p (T_{sat} - T_f)/h_{fg}$
Chong <i>et al.</i> (2015a)	$0.3866B^{-0.8} (G/G_m)^{0.78} (\varepsilon/\varepsilon')^2$	$c_p (T_{sat} - T_f)/h_{fg}$
Qiu <i>et al.</i> (2015)	$0.32B^{-0.8} (G/G_m)^{0.95} (\varepsilon/0.577)^{0.38}$	$c_p (T_{sat} - T_f)/h_{fg}$
Wang <i>et al.</i> (2017a)	$0.2674B^{-1} Ma^{0.5}$ $0.5075B^{-0.7114} Ma^{0.713}$	$c_p (T_{sat} - T_f)/h_{fg}$

fraction on the air-steam mixture, and the effect of nozzle size. Direct visualization techniques will be employed using a high-speed camera.

2 EXPERIMENTAL SET-UP AND IMAGE PROCESSING METHOD

2.1 Description of experimental set-up

Figure 1 shows a schematic diagram of the experimental facility that discharges a mixture of air and steam into a rectangular pool with subcooled water. During the experiments, the water in the pool and to generate the steam was filtered and treated by a reverse osmosis system to avoid possible impurities and reduce hardness. The pool has all its walls transparent to allow optical flow measurement, its dimensions are (length × width × height) 1500 mm × 500 mm × 600 mm [20].

In the experiment the water level was kept at 500 mm. The injection height was performed at 100 mm from the bottom of the pool using two interchangeable stainless-steel nozzles with different inner diameters (5, 6 mm). This was chosen because it is the nozzle diameter range used by many authors [4, 10, 18, 21–25].

Compressed air is injected through a screw air compressor with a flow rate of 1.42 m³/min and a maximum working pressure of 10 bar. Immediately downstream of the compressor, an air tank is used to stabilize the air conditions before injection. A flow meter is then used for measurement, which has an operating range of 50–500 l/min and a maximum pressure of 7.5 bar. The air is heated above steam temperature by two heaters in parallel to avoid steam condensation during mixing. For each heater, the temperature is controlled by a closed-loop PID control system and a power module. The temperature at the heater outlet is measured with a type ‘K’ thermocouple and is used as set point for the control.

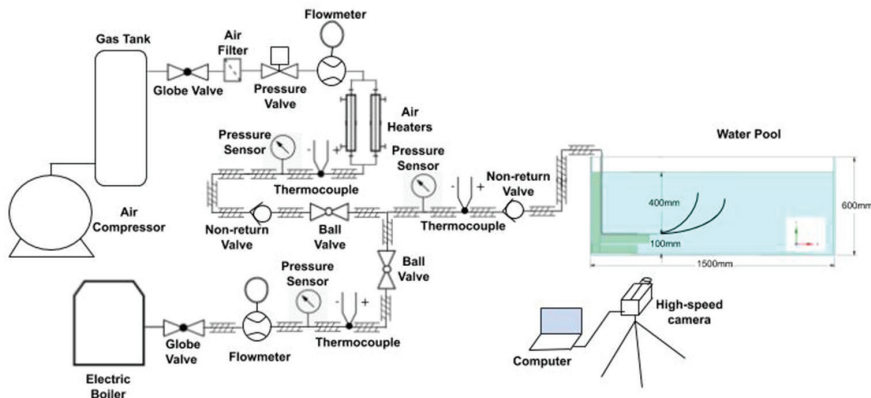


Figure 1: Schematic diagram of the facility [20].



Figure 2: Photograph showing the experimental set-up [20].

An electric steam boiler with a maximum working pressure of 6.5 bar is used in the steam line and the discharged flow rate is controlled by a flowmeter with a working range of 50–400 l/min. Pressure and temperature sensors are placed before the steam mixes with the air and just before the injection nozzle. All sensors are connected to a data acquisition system operated by a Labview Software (see Fig. 2).

To obtain a clear image, a LED panel was placed behind the pool as a backlight. The jet behavior was recorded with the PCO.1200 hs high-speed camera, whose technical characteristics allow obtaining clean images of moving objects, in addition to having the capability of acquiring a high number of images per second.

2.2 Experimental initial conditions

Table 2 shows the initial conditions of the series of experiments carried out. The following quantities were varied: air volumetric fraction injected into the pool, nozzle diameter and nozzle exit velocity.

Table 2: Initial conditions of the series of experiments [20].

Nozzle diameter (mm)	Nozzle exit velocity (m/s)	Air volumetric fraction, V_a
5	125, 175, 225	0.25, 0.5, 0.75, 1
6	125, 175, 225	0.25, 0.5, 0.75, 1

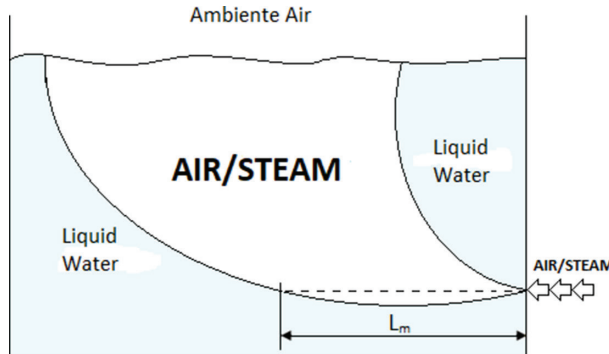


Figure 3: Behavior of a horizontal gas jet into liquid ambient.

2.3 Characterization of horizontal jet

The horizontal jet flow can usually be separated into two zones: momentum jet and buoyant jet. In the first zone, the shape of the jet keeps practically straight due to its high velocity. Whereas that the second regime, the buoyancy force causes the jet to move towards the free surface and the jet takes the form of a plume. This work will focus on determining the momentum length (L_m). The momentum length (L_m) is the length from the nozzle exit to the intersection with the gas–liquid boundary (Fig. 3).

2.4 Image processing method

For the image processing, a reference image (background) of 1024×1280 pixels without jet discharge is obtained for each one of the nozzles, which will be used to obtain the number of pixels per millimeter by taking the outer nozzle diameter as a frame of reference. This image also provides the location of the nozzle outlet that is used to calculate the momentum length. For this study, the maximum number of frames that the camera could take before filling the RAM memory was 817, this was determined by the resolution and exposure time selected on the camera software.

The images obtained by the camera are processed in MATLAB using a multistep routine, whose major steps are described below. First, the crop out the original image to remove the uninteresting parts in the research (see Fig. 4a). A binary image is then created from the two-dimensional grayscale image using a given threshold method (see Fig. 4b). Subsequently, median filtering of the image is performed where each output pixel contains the median value around the corresponding pixel in the input image (see Fig. 4c). A function is used to fill holes in the input binary image for the areas within the jet that cannot be

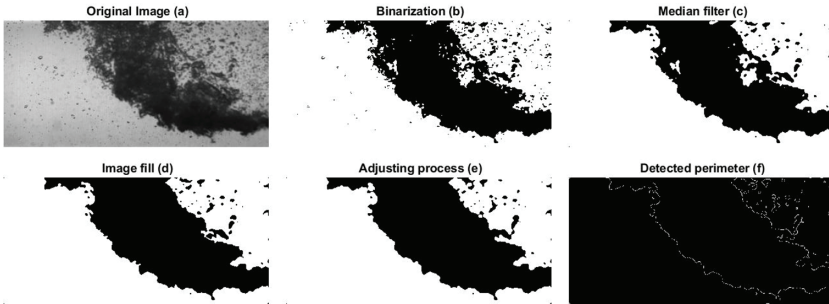


Figure 4: Routine realized in MATLAB to determine the jet interface.

reached by filling the background from the edge of the image (see Fig. 4d). Then, two functions perform morphological adjustment to eliminate small bubbles that do not provide much information to the study (see Fig. 4e). The last step is a function that returns a binary image with the perimeter pixels (see Fig. 4f) [20].

Although in our experiment the jet pinch-off phenomenon is not appreciated because it is discharged at high velocities into the pool. Within the images processing, the jet pinch-off phenomenon in its trajectory from the nozzle to the free surface. Concisely, it is obtained by linearizing the jet perimeter, i.e., for each x-coordinate, there can be only one y-coordinate.

2.5 Measurement uncertainty analysis

In this experimental system, the uncertainty of measurement is determined by the sensors errors, the photos acquisition using the camera and the processing of these images in MATLAB. The accuracies of steam flow meter, air flow meter, pressure sensors and K-type thermocouples are 2.5%, 2%, 0.25% and 0.4%, respectively.

The images obtained by the high-speed camera have a resolution of 1024×1280 pixels, where each millimeter corresponds to approximately 3 pixels, which would be an error in the spatial resolution of the image of 0.6 mm, i.e., an uncertainty of less than 1%. The maximum number of images obtained is 817 consecutive images, which depends on settings in the camera configuration, such as selected resolution and exposure time.

During the processing of the images obtained by MATLAB, after performing all the steps (threshold method to obtain the grey scale image, median filter, fill function, morphological adjustment and detected perimeter) is less than 2%.

The average momentum length (L_m) is obtained by taking the arithmetic average of the 817 consecutive images measured. The random error of these continuous images is calculated by the standard deviation.

$$L_m = \frac{1}{817} \sum_{i=1}^{817} L_m(i) \quad (1)$$

$$s_n = \sqrt{\frac{\sum (L_m(i) - \bar{L})^2}{(817 - 1)}} \quad (2)$$

The accidental or random error (ε_{random}) is evaluated from 3 sets ($N = 3$) of measurements of 817 images each, by means of the Standard Error of the Mean ($\frac{1}{2}$ of the confidence interval). A MATLAB script processes measurement data, and the random error is calculated for each test.

3 EXPERIMENTAL RESULTS AND DISCUSSION

After obtaining all the images for each of the programmed experiments, the digital processing of these images is carried out to characterize the discharged flow. The experimental results obtained for each of the initial conditions are shown in Table 3. A sampling has been done with the two nozzles varying the flow rate for different air volumetric fractions. The volumetric flow of the air-steam mixture was varied from 150 l/min to 380 l/min taking the air volumetric fraction of 0.25, 0.5, 0.75 and 1. Dimensionless Reynolds, Mach and Froude numbers are determined based on nozzle outlet parameters. In the table, P_m and T_m are the absolute pressure and temperature upstream of the nozzle outlet, respectively.

In some cases, the air fraction does not exactly match the previously predicted value because it is highly dependent on the steam fraction. The values of the air volumetric fraction are obtained from the data reported by the acquisition of the air flow meter and steam flow meter, and then obtaining the percentages, respectively.

As mentioned earlier, many authors give the momentum jet length as a function of Froude number:

$$Fr = \frac{u_e}{\sqrt{g(\Delta\rho/\rho_g)D}} \quad (3)$$

where u_e nozzle exit velocity, g gravity acceleration, $\Delta\rho$ is the subtraction of water density (ρ_l) and gas density (ρ_g) and D is the nozzle inner diameter. The gas density is the weighted average obtained from the total mass and total volumetric flow rate. Considering a homogeneous mixture, the mass is calculated from the volumetric flow rate and specific gravity of each fluid.

The Reynolds number is another dimensionless number that considers other essential parameters that relate the inertial conditions of the fluid, such as velocity and characteristic length of the problem (in our case is nozzle inner diameter) to the viscous forces, so it considers the conditions of the fluid itself, which depend largely on the air fraction and steam. Equation (4) show how Reynolds number is calculated, where ν is kinematic viscosity of the fluid.

$$Re = \frac{u_e D}{\nu} \quad (4)$$

Another dimensionless number that can provide important information in the study is the Mach number (eqn (5)), which allows to non-dimension the speed of the jet with respect to the sound speed (u_s). Normally, the conditions of the jet at the nozzle are used, since it could be determined if the flow is choked (If $M = 1$ there will be choked flow), which would indicate that the maximum flow that can pass through the duct has been reached. Mach number is defined by eqn (5):

$$M = \frac{u_e}{u_s} \quad (5)$$

Table 3: Experimental results for each initial conditions.

<i>D</i>	<i>V_a</i>	<i>Fr</i>	<i>Mach</i>	<i>P_m</i>	<i>ρ_g</i>	<i>T_m</i>	<i>ṁ</i>	<i>u_e</i>	<i>Re</i>
(mm)				(Pa x 10 ⁵)	(kg/m ³)	(K)	(x 10 ⁻³ kg/s)	(m/s)	(x 10 ⁵)
5	1	20.57	0.343	1.24	1.28	356.10	3.19	127.26	0.37
5	0.63	23.21	0.268	1.83	1.55	380.96	2.93	130.19	0.54
5	0.45	20.81	0.242	1.59	1.23	378.79	1.83	130.64	0.48
5	0.26	18.88	0.216	1.47	1.04	379.64	1.00	128.90	0.44
5	1	30.8	0.468	1.51	1.54	370.24	5.28	174.64	0.61
5	0.77	33.22	0.366	2.27	2.01	383.07	5.50	164.63	0.82
5	0.53	29.92	0.326	1.93	1.52	381.04	3.32	169.89	0.72
5	0.27	27.66	0.292	1.74	1.21	383.62	1.60	175.98	0.70
5	1	43.22	0.603	1.81	1.83	380.67	8.13	225.82	0.93
5	0.73	45.95	0.481	2.47	2.12	381.67	7.64	222.87	1.18
5	0.52	37.03	0.396	2.01	1.57	379.97	4.14	208.39	0.92
5	0.25	45.87	0.358	3.05	2.03	404.26	3.21	226.64	1.47
6	1	18.02	0.341	1.20	1.29	369.00	4.51	123.71	0.44
6	0.79	17.91	0.282	1.41	1.35	369.83	3.96	120.19	0.48
6	0.5	16.24	0.238	1.31	1.07	371.12	2.33	121.85	0.45
6	0.25	13.94	0.199	1.18	0.84	372.23	1.01	118.26	0.40
6	1	27.06	0.481	1.38	1.49	376.63	7.31	174.14	0.68
6	0.74	28.98	0.401	1.69	1.55	370.34	6.60	182.21	0.85
6	0.47	26.61	0.351	1.58	1.27	374.87	3.94	184.94	0.81
6	0.25	22.68	0.307	1.32	0.93	379.43	1.70	183.84	0.68
6	1	37.48	0.620	1.60	1.74	384.97	11.02	224.02	1.03
6	0.77	36.79	0.503	1.87	1.74	372.57	9.20	219.51	1.13
6	0.52	33.16	0.429	1.71	1.40	374.51	5.59	220.25	1.04
6	0.25	33.31	0.379	1.85	1.32	387.08	2.99	227.71	1.18

3.1 Momentum length of the gas jet

With all continuous images, an image with variable spatial intensity is obtained using a summation method in MATLAB, where each processed image is summed to the last one. Figure 5(a-d) show how the discharge behaves at the velocity of 125 m/s and diameter of 6 mm for 4 air volume fractions. The contour colors show how many times in the images a specified place in the vision field is occupied by the mixture of air-steam.

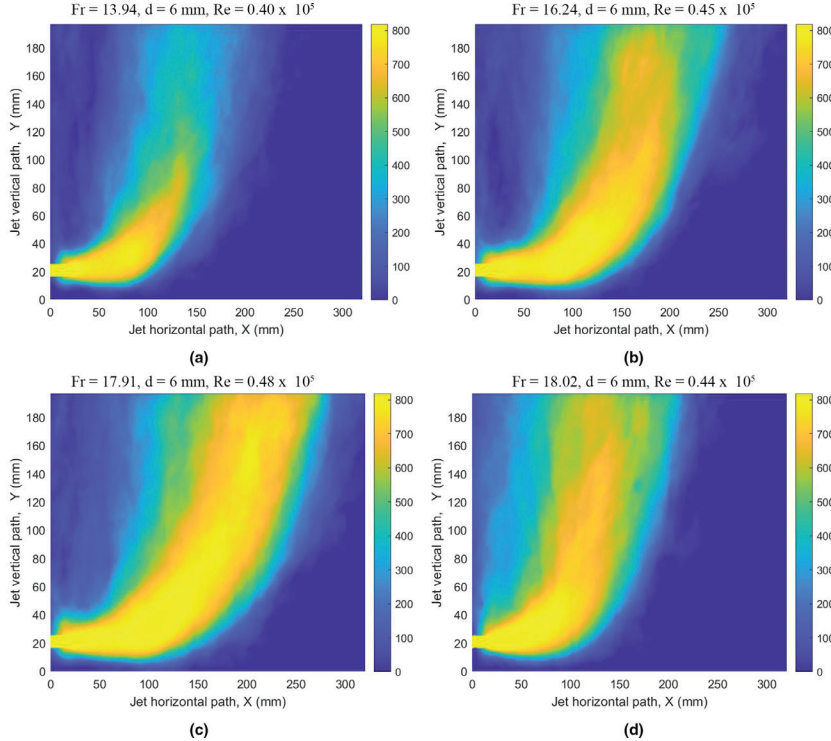


Figure 5: Experimental results for horizontal buoyant jets in stagnant water (a) $V_a = 0.25$, (b) $V_a = 0.5$, (c) $V_a = 0.79$, (d) $V_a = 1$.

In the case that we have the lowest velocity, and the air fraction is 0.25 (Fig. 5a), we can appreciate very well how the steam condenses while jet rises in the upward plume. This is because the velocity is so small that the buoyancy force prevails over the momentum force. For air fraction of 0.5 and 0.79 (Fig. 5b–c), there is a noticeable difference in the upward plume, because when the jet is 79% air it is observed that it occupies a larger space for many images, which is related to the lower percentage of steam that condenses. In Fig. 5d, the momentum force that determines the presence of steam disappears and only the buoyancy force is present, which is why the momentum jet length is so small.

3.2 Effect of air volumetric fraction on the dimensionless momentum length

The penetration length of the horizontally discharged jet is determined by several phenomena. First, as the amount of air in the mixture increases, buoyancy forces become dominant and heat transfer by direct contact of the steam with the water deteriorates. Conversely, increasing the amount of steam, the momentum forces are favored that allows a greater momentum length to exist. In addition, the entrainment/deposition balance on the gas-liquid interface is strongly influenced by the jet-pool velocity differences, since higher values of velocity would lead to higher the turbulence, which in turn produces a higher droplet entrainment at the gas-liquid interface. This higher entrainment causes a loss in the amount of motion of the jet, effect which is also increased by the fact that the droplets must be accelerated by the jet stream to values close to its velocity. In addition, these entrained droplets (which are

at pool temperature) will absorb energy from the jet that will favor the condensation of the steam contained in the jet. Therefore, both effects tend to reduce the penetration length of the jet, but only the second phenomenon affects the steam. Also, at the gas–liquid interface, steam condensation is favored (difference in temperature), but at the same time, due to steam condensation, the non-condensable will tend to melt towards this zone, which will reduce the condensation effect which will be favored with the increase in the volume fraction of non-condensable gases. Additionally, the increase of the inlet velocity/flow rate is associated with a higher discharge pressure, which in turn causes the expansion at the nozzle outlet to be greater (expansion to equalize the pressure of the jet with that of the surrounding medium). The higher the pressure, the greater the expansion (greater the expansion angle and over a greater length), and the expansion coefficients of non-condensable and steam are different. Therefore, as a consequence of the described above, there will not be a unique cause–effect relationship with the combination of the described phenomenology, so that there will be a series of phenomena that interfere with each other.

In general lines, Fig. 6 shows that as the air volume fraction increases there is a decreasing tendency of the penetration length. However, for the two low injection velocities this trend is not clear, presenting constant values or even a slight upward trend up to air volume fractions of 0.6–0.8. These trends can be explained by the interference between the different phenomena explained above (diffusion of non-condensable to the gas–liquid interface, balance of droplet entrainment-deposition, pressure effect, etc.). All these factors result in a complex interaction of the different phenomena, which leads to the fact that there is no single phenomenon that predominates over the rest in all the conditions analyzed, but rather a complex balance of these phenomena that changes depending on the conditions analyzed.

3.3 Effect of velocity on the dimensionless momentum length

Figure 7a–d shows the effect of velocity on the dimensionless momentum length in the two nozzles for the air fractions studied. With increasing velocity, the dimensionless momentum length increases for all four air fractions, which is caused by the fact that the transition point to the buoyancy-controlled regime is shifted further, downstream of the nozzle outlet (increase of buoyancy forces with the increase of the non-condensable gas volumetric fraction). When the air fraction is 0.25 and velocity 225 m/s (see Fig. 7a), the longest momentum length is obtained, this could probably be explained by the fact that the increase in velocity leads to an increase in the percentage of steam in the mixture and therefore the condensation of the steam makes the length longer. Furthermore, at this point the pressure is highest, which results in a higher expansion angle. This expansion angle is determined by the need

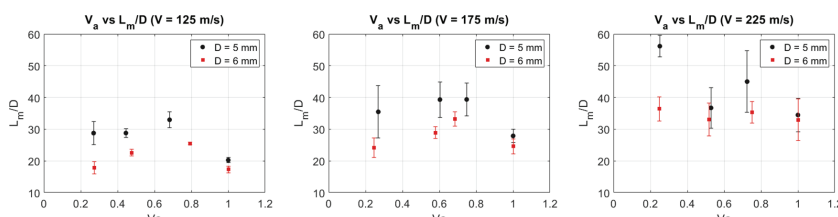


Figure 6: Effect of air volumetric fraction on the dimensionless momentum length (a) Velocity = 125 m/s, (b) Velocity = 175 m/s, (c) Velocity = 225 m/s.

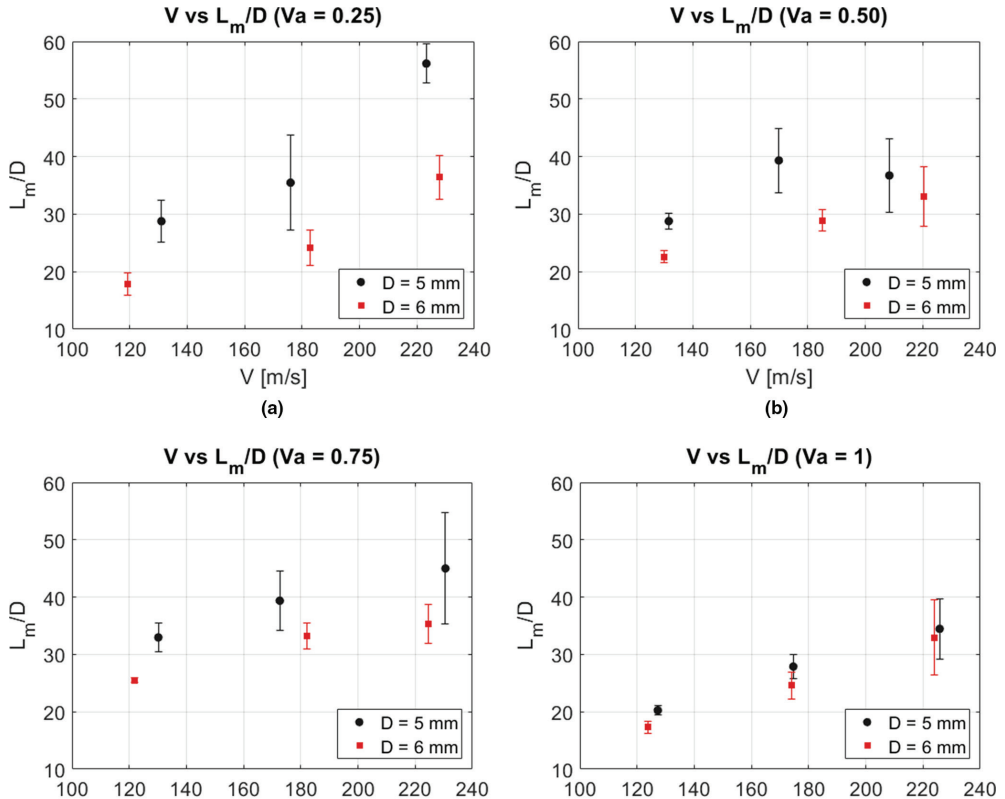


Figure 7: The influence of velocity on the momentum length (a) $V_a = 0.25$, (b) $V_a = 0.5$, (c) $V_a = 0.75$, (d) $V_a = 1$.

of the jet to equalize its pressure with the pressure of the fluid where it is discharged, which results in a predominance of the momentum force and thus an increase in the momentum length.

When there is an air jet, i.e., when the volume fraction of air is equal to 1 (Fig. 7d), the smallest momentum length is obtained for all velocities compared to the cases when steam was present. This phenomenon is a consequence of the absence of steam, which means that air buoyancy predominates over air momentum forces, due to the densities difference.

3.4 Correlation for predicting dimensionless momentum length

The dimensionless momentum length into stagnant water is governed by several parameters, such as the flow velocity, the fluid density, the nozzle area, and the percentage of air-steam mixture. These parameters can be encompassed in non-dimensional numbers that allow standardized correlations to be obtained. The study considered several non-dimensional numbers, such as: Reynolds number, Froude number and Mach number. Another factor that was considered was the air fraction to account for the phenomena that appear when studying an air-steam mixture jet.

The fits were made using a MATLAB function, where some adjustment coefficients were also obtained by combining the non-dimensional numbers and the parameters described above using a linear regression in log scale to achieve the best possible approximation.

For dimensionless momentum length, the appropriate correlation is:

$$\frac{L_m}{D} = 0.2539 Fr^{1.2192} M^{-0.7227} \quad (6)$$

As can be seen in eqn (6), the dimensionless most appropriate momentum length correlation only depends on the Froude and the Mach numbers. Pearson product-moment correlation coefficient has a value of $R^2 = 0.952$, which can be considered as satisfactory for the values of our experiment.

The Fig. 8 shows the relationship of the dimensionless momentum length correlation to the experimental results. Error bands of ± 5 and $\pm 20\%$ are included to graphically appreciate the dispersion of the points. Just over 50% of the data points are within the -5% to $+5\%$ error band. While almost all the remaining points are within the -20% to $+20\%$ error band, only one point is outside the band, but very close.

3.5 Momentum length prediction through other correlations

The correlation obtained considers several variables that adjust the measurements carried out with the best possible correlation coefficient. On the other hand, there are more correlations obtained by other authors in different conditions, even with different fluids. The possibility of verifying the correlation behavior with external experimental data is not viable due to the lack of information about the conditions of the experiments. This fact has led to focus the study to the comparison of the predictions of different correlations, being able to evaluate the error obtained depending on the specific conditions of each one of them. Table 4 shows the correlations considered to study their predictions.

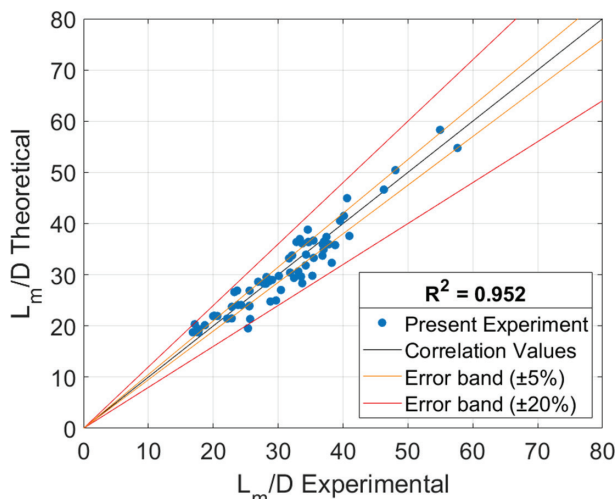


Figure 8: Comparison of calculated dimensionless momentum length and experimental measurements.

Table 4: Correlations considered to study.

Authors	Correlations	Fluid (gas/liquid)	Conditions
K. Harby	$\frac{L_m}{L_Q} = 2.29 \left(\frac{u_e^2}{gD} \frac{\rho_g}{\rho_l - \rho_g} \right)^{0.305}$	Air / Water	D=2–5mm M=0.59–1.05
Weichao Li	$\frac{L_m}{D} = 0.701 W_a^{-1936} \left(\frac{u_e^2}{gD} \frac{\rho_g}{\rho_l} \right)^{0.5046}$	Steam-Air mixture / Water	P _{in} =0.1–0.5 MPa W _a =0.025–07
J. L. Carreau	$\frac{L_m}{D} = 1.34 \left(\frac{u_e^2 (P_g - P_l)}{D} \frac{\rho_g}{\rho_l - \rho_{g,amb}} \right)^{0.39}$	Nitrogen / Water	D=0.3–1mm P _{in} =0.5–10 MPa sonic
Hoefele and Brimacombe	$\frac{L_m}{D} = 10.7 \left(\frac{u_e^2}{gD} \frac{\rho_g}{\rho_l} \right)^{0.46} \left(\frac{\rho_g}{\rho_l} \right)^{0.35}$	Air, Argon and Helium / Mercury, Zinc-chloride solution and Water	D=2–4.7mm $\rho_g u_e = 20 – 1800 \text{ kg/m}^2\text{s}$
Ji Ma	$\frac{L_m}{D} = \log \left(\frac{u_e^2}{gD} \frac{\rho_g}{\rho_l - \rho_g} \right) Re^{0.198}$	Air / Fresh water and Salt water	D=3–6mm Q=3–200 slm

In these correlations the Froude number is broken down due to the different definitions of it that are used. Other parameters, such as air mass fraction (W_a) or pressure (P), appear in some of these equations. In the Harby correlation [18], L_m is divided by L_Q instead of D. In this case L_Q corresponds to the square root of the nozzle area. The trends of the calculations have been represented by the correlations against the experimental measurements, obtaining the Fig. 9.

These trends are linear and represent the relationship between the measurements made and the calculation through each correlation. There is an important dispersion of predictions regarding the different correlations exposed.

Apparently, the correlations that present less error are those that consider a greater variety of scenarios with respect to the fluids used. Hoefele and Brimaconbe [15], with three gas and three liquid, and Weichao Li [13], with air-steam as gas, have a correlation coefficient of 0.83 and 0.87, respectively. The other authors have a greater error in their prediction but only consider non-condensable gas discharges in water. It is possible that a larger sample of fluids has better capabilities. The eqn (6) obtains the best approximation because the correlation has been obtained from the exposed experimental measurements, but the trend is like the Hoefele and Li prediction, which is apparently the good behavior.

Non-condensable gas discharges in subcooled water seem to depend largely on the surrounding conditions. The Carreau experiment [16], in a range of very high pressures and sonic velocities, or Harby [18], with high Mach numbers, have very different conditions and greater errors appear.

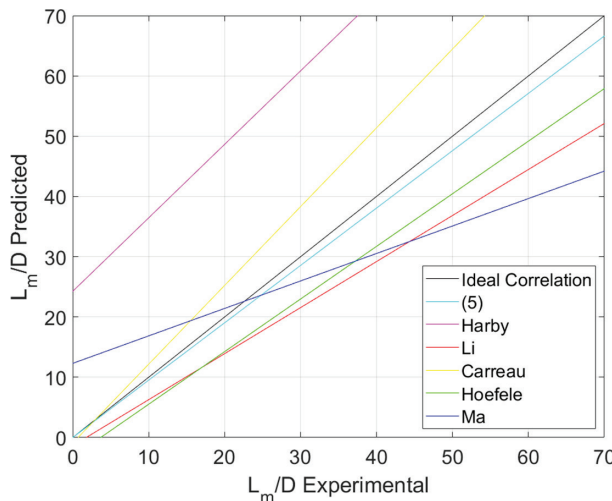


Figure 9: Trend of momentum length prediction values with respect to the nozzle diameter with different correlations.

4 CONCLUSIONS

The work carried out has characterized the behavior of air and steam discharge in a pool with subcooled water for two nozzle diameters by varying the fraction of air in the mixture and the velocities of the gas mixture. The following conclusions were reached:

1. The phenomenology involved in the discharge of jets of mixed air and steam is complex and has a significant dependence on the inertial forces and properties of the fluid, such as its composition.
2. The effect of buoyancy forces has a different behavior for pure air jets and for air-steam mixture jets, being an important characteristic the influence by direct contact condensation suffered by the steam.
3. It has been found that the combination of Froude and Mach numbers gives the highest correlation coefficient for the correlation of the dimensionless length on the jet momentum.
4. Pearson product-moment correlation coefficient has a value of $R^2 = 0.952$, which can be considered satisfactory for the values of our experiment. The discrepancy between experimental results and theoretical results obtained through the correlation is within $\pm 20\%$.
5. The use of other correlations for the experimental measures presented offers an important dispersion. Correlations obtained using a major variety of fluids give results with assumable errors, but correlations obtained using non-condensable discharges into sub-cooled water give results for more restricted conditions.

ACKNOWLEDGEMENTS

The authors would like to acknowledge the support provided through the Spanish project EXMOTRANSIN ENE2016-79489-C2-1-P and the Santiago Grisolía Program for the training of research personnel.

REFERENCES

- [1] Kim, Y.S., Park, J.W. & Song, C.H., Investigation of the stem-water direct contact condensation heat transfer coefficients using interfacial transport models. *Int. Commun. Heat Mass Transf.*, **31**(3), pp. 397–408, 2004. <https://doi.org/10.1016/j.icheatmas-transfer.2004.02.010>
- [2] Stanford, L.E. & Webster, C.C., Energy Suppression and fission product transport in pressure-suppression pools, 1972.
- [3] Kerney, P.J., Faeth, G.M. & Olson, D.R., Penetration characteristics of a submerged steam jet. *AIChE J.*, **18**(3), pp. 548–553, 1972. <https://doi.org/10.1002/aic.690180314>
- [4] Chun, M.-H., Kim, Y.-S. & Park, J.-W., An investigation of direct condensation of steam jet in subcooled water. *Int. Commun. Heat Mass Transf.*, **23**(7), pp. 947–958, 1996. [https://doi.org/10.1016/0735-1933\(96\)00077-2](https://doi.org/10.1016/0735-1933(96)00077-2)
- [5] Kim, H.Y., Bae, Y.Y., Song, C.H., Park, J.K. & Choi, S.M., Experimental study on stable steam condensation in a quenching tank. *Int. J. Energy Res.*, **25**(3), pp. 239–252, 2001. <https://doi.org/10.1002/er.675>
- [6] Sun, L., Shi, E., Hao, R., Hu, S. & Wang, C., Experiment research on characteristic of steam plume of sonic submerged jet. *At. Energy Sci. Technol.*, **52**(5), pp. 834–838, 2018. <https://doi.org/10.3139/124.190036>
- [7] Meng, Z., Zhang, W., Liu, J., Yan, R. & Shen, G., Experimental study on the condensation of sonic steam in the underwater environment. *Nucl. Eng. Technol.*, **51**(4), pp. 987–995, 2019.
- [8] Weimer, J.C., Faeth, G.M. & Olson, D.R., Penetration of vapor jets submerged in subcooled liquids. *AIChE J.*, **19**(3), pp. 552–558, 1973. <https://doi.org/10.1002/aic.690190321>
- [9] Wu, X.Z., Yan, J.J., Shao, S.F., Cao, Y. & Liu, J.P., Experimental study on the condensation of supersonic steam jet submerged in quiescent subcooled water: Steam plume shape and heat transfer. *Int. J. Multiph. Flow*, **33**(12), pp. 1296–1307, 2007. <https://doi.org/10.1016/j.ijmultiphaseflow.2007.06.004>
- [10] Chong, D., Zhao, Q., Yuan, F., Wang, W., Chen, W. & Yan, J., Research on the steam jet length with different nozzle structures. *Exp. Therm. Fluid Sci.*, **64**, pp. 134–141, 2015. <https://doi.org/10.1016/j.expthermflusci.2015.02.015>
- [11] Qiu, B., Yan, J., Liu, J. & Chong, D., Experimental investigation on pressure oscillation frequency for submerged sonic/supersonic steam jet. *Ann. Nucl. Energy*, **75**, pp. 388–394, 2015. <https://doi.org/10.1016/j.anucene.2014.08.055>
- [12] Wang, F. et al., Shape feature and condensation heat transfer of supersonic steam jet in subcooled water. *Dongli Gongcheng Xuebao/Journal Chinese Soc. Power Eng.*, **37**(11), pp. 918–924, 2017.
- [13] Li, W., Meng, Z., Sun, Z., Sun, L. & Wang, C., Investigations on the penetration length of steam-air mixture jets injected horizontally and vertically in quiescent water. *Int. J. Heat Mass Transf.*, **122**, pp. 89–98, 2018. <https://doi.org/10.1016/j.ijheatmasstransfer.2018.01.075>
- [14] Igwe, B.U.N., Ramachandran, S. & Fulton, J.C., Jet penetration and liquid splash in submerged gas injection. *Metall. Trans.*, **4**(8), pp. 1887–1894, 1973. <https://doi.org/10.1007/bf02665417>
- [15] Hoefele, E.O. & Brimacombe, J.K., Flow regimes in submerged gas injection. *Metall. Trans. B*, **10**(4), pp. 631–648, 1979. <https://doi.org/10.1007/bf02662566>

- [16] Carreau, J.L., Roger, F., Loukarfi, L., Gbahoue, L. & Hobbes, P., Penetration of a horizontal gas jet submerged in a liquid. In *Proceedings of the Intersociety Energy Conversion Engineering Conference*, 1986, pp. 315–319.
- [17] Emani, A. & Briens, C., Study of downward gas jets into a liquid. *AIChE J.*, **54**(9), pp. 2269–2280, 2008. <https://doi.org/10.1002/aic.11524>
- [18] Harby, K., Chiva, S. & Muñoz-Cobo, J.L., An experimental investigation on the characteristics of submerged horizontal gas jets in liquid ambient. *Exp. Therm. Fluid Sci.*, **53**, pp. 26–39, 2014. <https://doi.org/10.1016/j.expthermflusci.2013.10.009>
- [19] Rassame, S., Hibiki, T. & Ishii, M., Void penetration length from air injection through a downward large diameter submerged pipe in water pool. *Ann. Nucl. Energy*, **94**, pp. 832–840, 2016. <https://doi.org/10.1016/j.anucene.2016.04.046>
- [20] Cordova, Y., Rivera, Y., Blanco, D., Berna, C., Muñoz-Cobo, J.L. & Escrivá, A., Experimental investigation of submerged horizontal air–steam mixture jets into stagnant water. *Adv. Fluid Mech. XIII*, **1**, pp. 89–101, 2020.
- [21] Simpson, M.E. & Chan, C.K., Hydrodynamics of a Subsonic Vapor Jet in Subcooled Liquid. *J. Heat Transfer*, **104**, p. 271, 1982.
- [22] Wu, X.-Z., Yan, J.-J., Li, W.-J., Pan, D.-D. & Chong, D.-T., Experimental study on sonic steam jet condensation in quiescent subcooled water. *Chem. Eng. Sci.*, **64**, pp. 5002–5012, 2009.
- [23] Harby, K., Chiva, S. & Muñoz-Cobo, J.L., Modelling and experimental investigation of horizontal buoyant gas jets injected into stagnant uniform ambient liquid. *Int. J. Multiph. Flow*, **93**, pp. 33–47, 2017.
- [24] Zhao, Q., Chen, W., Yuan, F., Wang, W., Chong, D. & Yan, J., Pressure oscillation and steam cavity during the condensation of a submerged steam jet. *Ann. Nucl. Energy*, **85**, pp. 512–522, 2015.
- [25] Zhao, Q., Cong, Y., Wang, Y., Chen, W., Chong, D. & Yan, J., Effect of non-condensation gas on pressure oscillation of submerged steam jet condensation. *Nucl. Eng. Des.*, **305**, pp. 110–120, 2016.